ARTICLE

Hydrodynamic Transformation of a Freestanding Polymer Nanosheet Induced by a Thermoresponsive Surface

Toshinori Fujie,[†] Jin Young Park,[‡] Atsushi Murata,[†] Nicel C. Estillore,[‡] Maria Celeste R. Tria,[‡] Shinji Takeoka,[*,†,§] and Rigoberto C. Advincula[‡]

Department of Life Science and Medical Bioscience, Graduate School of Advanced Science and Engineering, Waseda University (TWIns), 2-2 Wakamatsu-cho, Shinjuku-ku, Tokyo 162-8480, Japan, Departments of Chemistry and Chemical Engineering, University of Houston, Houston, Texas 77204-5003, and Consolidated Research Institute for Advanced Science and Medical Care, 513 Wasedatsurumaki-cho, Shinjuku-ku, Waseda University, Tokyo 165-0041, Japan

ABSTRACT Freestanding quasi-two-dimensional ultrathin films (e.g., 41 nm thick polymer nanosheets) were produced, on which stimuli-responsive 47 nm thick polymer brushes were constructed by atom transfer radical polymerization (ATRP) of poly(*N*-isopropylacrylamide). The resulting surfaces of the multilayered polysaccharide ultrathin films were evaluated by ellipsometry, IR imaging, in situ variable-temperature atomic force microscopy (AFM), and contact angle measurements. The morphological transformation of the freestanding polymer nanosheet bearing thermoresponsive polymer brushes was observed macroscopically through reversible structural color changes at the air−water interface. The dynamic shape change of the nanosheet was also monitored with the addition of a surfactant such as sodium *n*-dodecylsulfate to reduce the hydrophobicity of the surface. It was then demonstrated that the highly flexible freestanding polymer nanosheet is capable of acting as a unique platform for inducing stimuli-responsive behavior in nanomaterials.

KEYWORDS: polymer nanosheet • polysaccharide • layer-by-layer • atom transfer radical polymerization (ATRP) • thermoresponsive surface

INTRODUCTION

Stimuli-responsive surfaces have always been attractive objectives in materials science, from high-throughput sensing devices to molecular-driven actuators. The recent development of surface initiated polymerization (SIP) methods such as atom transfer radical polymerization (ATRP) (1) have made possible several useful applications of chemically surface modified nanomaterials. The surface modification of nanomaterials is expected to enhance their potential application in friction control (2), drug delivery (3), reversible thickness control (4), antireflection control (5), permeability control (6), and ion selectivity (7). Stimuli-responsive surfaces have been the subject of increasing interest over the past few years in the context of fundamental research and the development of commercial materials. The use of poly(*N*-isopropylacrylamide) (pNIPAM) is at the forefront of this research, due to the fact that it has a low critical solution temperature (LCST), which is readily observed at ∼32 °C (2, 3, 8, 9). In this case, the polymer chains undergo a change in conformation, a swollen-to-unperturbed coil transition, as the temperature is increased above the LCST. Hence, surface modification with pNIPAM provides a route to affecting the swelling and rheological properties of nanomaterials, a crucial step in their functionalization.

We have produced stimuli-responsive surfaces via the layer-by-layer (LbL) method (10–12). This method is an active area of focus for novel nanotechnology, useful for a wide variety of nanomaterials such as functionalized ultrathin films (i.e., nanosheets), including synthetic polyelectrolytes (10), biomacromolecules (13), colloid particles (14), and clays (15). The basic concept of the LbL method is the alternating deposition of oppositely charged polyelectrolytes via two mechanisms. The first and primary interaction is electrostatic; supportive interactions include hydrogen bonding, van der Waals interactions, and hydrophobic interactions (10, 16–18). Ultrathin LbL films that are suitable platforms for modifying various conjugates have been developed for electrochemical devices, chemical and biological sensors, nanomechanical sensors, nanoscale chemical and biological reactors, drug delivery systems, etc. (14, 19–21). Especially interesting applications of the LbL method have featured the construction of membrane-based three-dimensional structures such as core−shell colloidal particles and hollow capsules (22–24).

Thus far, quasi-two-dimensional freestanding LbL films having two accessible surfaces in one carrier have been produced (25–27); the example reported by Tsukruk et al. (28–30) has a large aspect ratio of over 10^6, a lateral dimension on the order of centimeters, and a thickness of

* To whom all correspondence should be addressed. Tel: +813-5369-7324. Fax: +813-5369-7324. E-mail: takeoka@waseda.jp.

Received for review February 19, 2009 and accepted June 2, 2009

[†] Graduate School of Advanced Science and Engineering, Waseda University (TWIns).

[‡] University of Houston.

[§] Consolidated Research Institute for Advanced Science and Medical Care, Waseda University.

DOI: 10.1021/am900111r

Published on Web 06/25/2009

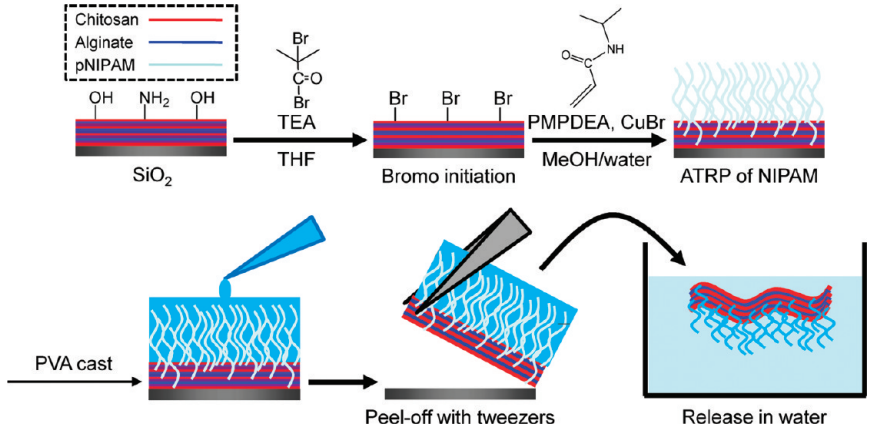

FIGURE 1. Procedure for preparation of a freestanding polysaccharide nanosheet bearing poly(*N*-isopropylacrylamide) brushes.

some tens of nanometers. The fabrication process was generally based on the LbL method with the addition of spin coating, or "spin coating assisted LbL (SA-LbL)" (31–33). The SA-LbL method is suitable for preparing an ultrathin film on a substrate which has been preliminarily covered with a sacrificial layer. In such a case, the dissolution of the sacrificial layer in appropriate solvents yields a freestanding ultrathin LbL film within several minutes. The SA-LbL method produces not only highly flat and smooth surfaces but also a versatile interface with optional charged or chemically activated groups. Since this approach to the fabrication of freestanding nanosheets has been established (28, 34, 35), the next target is to enhance the functionalization of the polymer nanosheets, such as the introduction of a stimuli-responsive surface.

The construction of stimuli-responsive surfaces on LbL films has been facilitated by employing surface initiated polymerization (SIP) techniques. In particular, the formation of polymer brushes via SIP has proven to be a successful novel approach utilizing pH-, photo-, and thermoresponsive polymers including pNIPAM, among other functional polymers (36, 37). The "grafting-from" or SIP approach has the benefit of placing initiating groups directly on the surface. This allows for good control over the grafting process. Various polymerization techniques have been developed for the preparation of pNIPAM brushes. Traditional free radical polymerization produces polymer brushes as layers up to 100 nm thick with high grafting density using immobilized initiators (azo, peroxide, or photoinitiators) on the surface. However, this chemistry offers poor controllability over the homogeneous brush length (approximately tens of nanometers) (38). This disadvantage can be overcome by the use of controlled living polymerization chemistry, such as atom transfer radical polymerization (ATRP), which is particularly suited for the preparation of homogeneous polymer brush surfaces on polymer nanosheets, since living polymerization utilizes fixed initiators.

In this study, we focus on the effect of thermoresponsive polymers such as pNIPAM on the hydrodynamics of freestanding polymer nanosheets. These sheets have unique physical properties, such as a large contact surface area and a flexibility derived from its huge size aspect ratio (39). For this purpose, we used polymer nanosheets composed of polysaccharides (40) as platforms to synthesize pNIPAM brushes. Although several methodologies have already been developed for pNIPAM using temperature-tuned materials such as ultrathin films or gels (41–43), we need to keep the freestanding ultrathin structure in a substrate-free condition in order to investigate the hydrodynamic properties of the polysaccharide nanosheets. To this end, we considered it necessary to maximize the interfacial contact area between the stimuli-responsive polysaccharide nanosheets bearing pNIPAM brushes (pNIPAM nanosheets) and the water surface to enhance its mobility. Hence, we decided to construct pNIPAM brushes on polysaccharide LbL films. This approach produces pNIPAM polymer brushes with a high grafting density; this is an ideal surface modification in order to obtain a large contact area with water molecules and is much preferred to conventional LbL films containing functional polymers that are internal to the structure.

In particular, this study demonstrates that it is possible to construct ultrathin, flexible, freestanding polymer nanosheets having surfaces functionalized with thermoresponsive polymer brushes via ATRP. Polysaccharide nanosheets were used with a thickness on the order of tens of nanometers (44, 45), composed of chitosan (polycation) and sodium alginate (polyanion). These polysaccharides have potentially chemically reactive groups in their chemical structures (amino and hydroxide groups), allowing for various ATRP initiators to be coupled with them in the presence of base (46, 47). Figure 1 describes the preparation of polysaccharide LbL films by the SA-LbL method, where the LbL films are functionalized with pNIPAM brushes by ATRP. A freestanding pNIPAM brushed polysaccharide nanosheet (pNIPAM nanosheet) was obtained using a supporting film method (48). The macroscopic hydrodynamic properties (e.g., thermoresponsive behavior, surface hydrophobicity in the presence of surfactants) of the resulting pNIPAM nanosheets suspended in water were investigated by changing the temperature and concentration of the surfactants.

EXPERIMENTAL SECTION

Materials. The polyelectrolytes chitosan (M_w = 88 kDa; deacetylation degree >80%) and sodium alginate (M_w = 106 kDa; approximate glucuronic/mannuronic ratio 1:1.3) were purchased from Nacalai Tesque, Inc. (Kyoto, Japan). Polyvinyl

alcohol (PVA; $M_w = 22$ kDa) was purchased from Kanto Chemical Co., Inc. (Tokyo, Japan). Silicon oxide (SiO_2) substrates (silicon wafers: 200 nm thick SiO_2 layers; boron doped; crystal face 100; p type) were purchased from KST World Co. (Fukui, Japan), cut into a convenient size (typically 4 cm^2), immersed in a mixture of sulfuric acid and hydrogen peroxide (3:1) for a 10 min washing, and then thoroughly rinsed with deionized (DI) water (18 MΩ cm). Triethylamine, 2-bromoisobutyryl bromide (2-BIB), CuBr, and *N*,*N*,*N*′,*N*″,*N*″-pentamethyldiethylenetriamine (PMDETA) were used as received from Tokyo Chemical Industry (TCI) Co. (Tokyo, Japan). *N*-Isopropylacrylamide (NIPAM), purchased from TCI, was purified by recrystallization from hexane. Sodium *n*-dodecylsulfate (SDS) was purchased from Kanto Chemical Co., Inc. (Tokyo, Japan).

Preparation of the Polysaccharide Nanosheet. All preparation routines for polysaccharide nanosheet fabrication were conducted in a clean room (class 10000 conditions) to avoid contamination. Chitosan (1 mg/mL, 1% (v/v) acetic acid) and Na alginate (1 mg/mL) solutions were prepared with DI water. A 1 mL solution of chitosan as a first layer was dropped onto the SiO_2 substrate, and the substrate was rotated at 4500 rpm (rpm) for 15−20 s. Then, the substrate was rinsed twice with DI water and dried by spinning (4500 rpm, 30 s). Subsequently, an SA-LbL of each polysaccharide (4500 rpm, 15 s for each polyelectrolyte) and a water rinse were alternatively performed. The process was terminated at the chitosan spin coating stage with 10.5 pairs of layers. After the surface was dried in vacuo, the polysaccharide LbL films on the SiO_2 substrate were subjected to initiator functionalization for ATRP.

Preparation of the pNIPAM Nanosheet. Surface functionalization of the polysaccharide LbL film was undertaken with a bromo initiator by following the method reported by Husson et al. (47), coupling the 2-BIB initiator with the hydroxide or amine group of chitosan. The polysaccharide LbL film on the SiO_2 substrate was immersed in a 50 mL flask containing 25 mL of a dry THF solution and 0.5 mL of triethylamine. The flask was placed in an ice bath, and the contents were gently stirred. Then, 0.5 mL of a liquid 2-BIB initiator was slowly added dropwise to the solution under an N_2 atmosphere. The flask was purged with N_2 gas and removed from the ice bath, and the reaction in the flask was allowed to continue at room temperature overnight. After the reaction was complete, the functionalized substrate was removed from the flask with tweezers, rinsed with THF and then DI water, and dried in vacuo overnight.

The ATRP conditions for NIPAM polymerization generally followed those in our previous report (37). Three Schlenk flasks were prepared for ATRP. The first Schlenk flask was charged with 25.4 mg (0.176 mmol) of CuBr and 111 μL (0.530 mmol) of PMDETA under a N_2 atmosphere. A second Schlenk flask was charged with 2 g (17.7 mmol) of NIPAM dissolved in 17.5 mL of water and 17.5 mL of methanol. As the concentration of NIPAM was changed from 0.1 to 0.5 M, the volumes of CuBr and PMDETA were adjusted by the stoichiometric mixing ratio corresponding to the NIPAM molar ratio. The surface-functionalized LbL substrate was placed in a third Schlenk flask. The mixture in the first Schlenk flask was transferred via cannula to the second Schlenk flask and mixed for 5 min, and this mixture was subsequently transferred to the third flask containing the LbL substrate. The polymerization was performed at room temperature from 0.5 to 4 h in order to evaluate the growth (thickness) of the pNIPAM brushes. After polymerization, the substrate was removed, thoroughly rinsed with DI water and methanol, and dried in vacuo overnight. Finally, the pNIPAM nanosheet was obtained using a water-soluble supporting film. A 10 wt % PVA aqueous solution was cast upon the pNIPAM nanosheet on the SiO_2 substrate and dried in vacuo. Then, the bilayered film of pNIPAM nanosheet and water-soluble PVA supporting film was peeled from the SiO_2 substrate with tweezers. Following immersion of the bilayered film in DI water, the freestanding pNIPAM nanosheet was obtained and photographed using a digital camera (Olympus C-5050 ZOOM, Olympus Co., Tokyo, Japan) for macroscopic observation.

Characterization of the pNIPAM Nanosheet. Ellipsometry was used to determine the thickness of the polysaccharide LbL film. All measurements were conducted using a null ellipsometer (Multiskop, Optrel, Berlin) operating in a polarizer-compensator-sample-analyzer mode. A He−Ne laser (λ 632.8 nm) acted as the light source at a 60° angle of incidence. A multilayer flat model was used to calculate the LbL thicknesses from the experimentally measured ellipsometric angles of Δ and Ψ, assuming a refractive index of 1.50 and 1.46 for the LbL films and 1.5 nm thick SiO_2 layer, respectively. The film thickness was then calculated using a fitting program (Elli, Optrel).

X-ray photoelectron spectroscopy (XPS) was carried out on a PHI 5700 instrument with a monochromatic Al Kα X-ray source (1486.6 eV) incident at 90° relative to the axis of a hemispherical energy analyzer. The spectrometer was operated at both high and low resolution with pass energies of 23.5 and 187.85 eV, respectively. Photoelectrons were collected at a takeoff angle of 45° from the surface and an analyzer spot diameter of 1.1 mm. The survey spectra were collected from 0 to 1400 eV, and the high-resolution spectra were obtained for C1s, O1s, N1s, Cu2p, and Br3d. All spectra were collected at room temperature with a base pressure of 1×10^{-8} Pa. Electron binding energies were calibrated with respect to the C1s line at 284.5 eV.

FT-IR imaging was performed on a Digilab Stingray imaging system consisting of a Digilab FTS 7000 spectrometer, a UMA 600 microscope, and a 32 × 32 mercury−cadmium−telluride IR imaging focal plane array (MCT-FPA) image detector with an average spatial area of 176 μm × 176 μm in transmission mode. An 8 cm^{-1} nominal spectral resolution and an undersampling ratio (UDR) of 4 for the imaging were set up, and spectral data were collected with 1240 scans. All image processing and data extraction were obtained using the Win-IR Pro 3.4 software package.

Atomic force microscopy (AFM; Agilent 5500 AFM/SPM System, Agilent Technologies) was used to investigate surface morphologies and perform surface analysis. The AFM measurements were carried out with a piezoscanner (maximum scan size 9 × 9 μm^2) at room temperature. Commercially available cantilever-style tapping mode tips (TAP300, Silicon AFM Probes, TedPella, Inc., CA) were used, with a resonance frequency in the range of 290−410 kHz. All images (AFM topography, tapping mode) were filtered and analyzed using the SPIP (Scanning Probe Image Processor, Imagemet.com) package. A temperature controller (321 Autotuning, Lakeshore) was used for temperature-driven in situ AFM scanning.

RESULTS AND DISCUSSION

Preparation of the pNIPAM Nanosheet. The polysaccharide LbL film, prepared directly on the surface of the SiO_2 substrate by the SA-LbL method, had a resulting ellipsometric thickness of 41 ± 0.33 nm with 10.5 polysaccharide layer pairs. The thickness is proportional to the number of layer pairs, as described in our previous reports (43, 44). The hydroxide or amino groups of the polysaccharide film on the substrate reacted with the liquid 2-BIB initiator, resulting in an ester or amide linkage. This surface functionalization was confirmed by XPS analysis. The narrow scan mode showed the presence of Br3d at 72 eV, originating from the bromo initiator. This peak was not observed in the LbL film prior to its functionalization (Figure 2a).

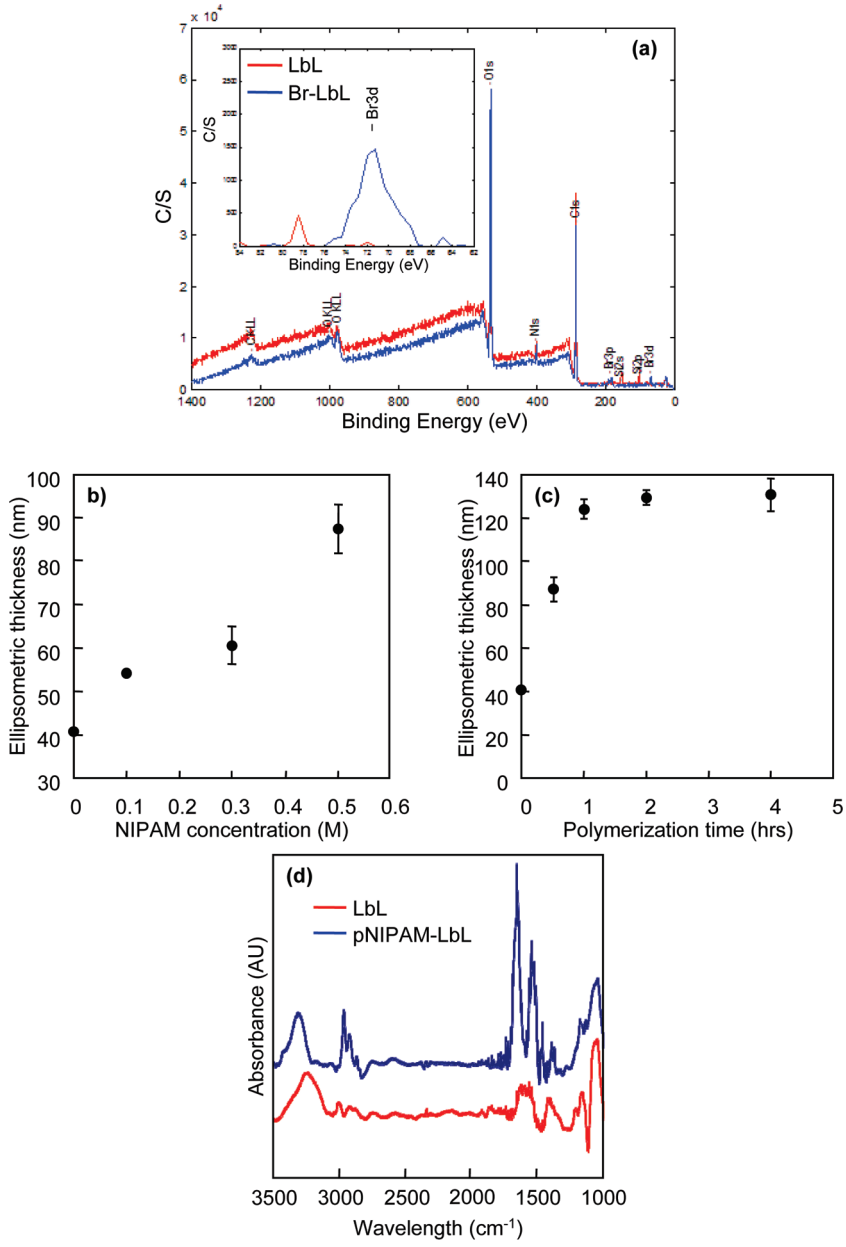

FIGURE 2. (a) Spectroscopic analysis of the pNIPAM nanosheet, with an XPS spectrum of the bromo-functionalized surface (red, polysaccharide nanosheet; blue, nanosheet after bromo initiation). (b, c) Ellipsometric thickness of the pNIPAM nanosheet on the SiO_2 substrate as a function of (b) NIPAM monomer concentration and (c) polymerization time. (d) FT-IR spectra of the pNIPAM nanosheet on the SiO_2 substrate (red, polysaccharide nanosheet; blue, pNIPAM nanosheet).

The effect on the ellipsometric thickness of the films (including a pNIPAM brushed layer and an LbL film) of varying the polymerization conditions (e.g., concentration, polymerization time) under which the NIPAM was polymerized on the polysaccharide LbL surface was evaluated. As the concentration of the NIPAM monomer increased, the ellipsometric thickness increased proportionally. At a NIPAM concentration of 0.5 M, the total film thickness reached 88 nm (thickness of pNIPAM brushes 47 nm) (Figure 2b).

For polymerization times over 1 h at a concentration fixed at 0.5 M, the total film thickness remained constant at 124 nm (pNIPAM brush thickness 83 nm) (Figure 2c). However, the surface of the pNIPAM brushed film became heterogeneous for reaction over 1 h. Therefore, we decided on using films with a optimized total film thickness of 88 nm (pNIPAM brushes, 47 nm; polysaccharide LbL film, 41 nm) produced with polymerization conditions of 0.5 M NIPAM concentration and 0.5 h polymerization time.

Furthermore, XPS analysis allowed us to clarify the elemental composition of the pNIPAM nanosheet on the SiO_2 substrate, in particular with respect to the degree of polymerization and the inclusion of CuBr salts during ATRP. A survey scan of the pNIPAM nanosheet showed peaks only for carbon, oxygen, nitrogen, and silicon (Figure S1, Supporting Information). The absence of a Cu2p peak (the XPS survey scan is available in the Supporting Information) indicates that the catalyst was successfully removed by postpolymerization rinsing. The FT-IR spectra have a strong methylene stretch centered at 3000 cm^{-1}, and the amide I carbonyl stretch is centered at 1650 cm^{-1}, derived from the

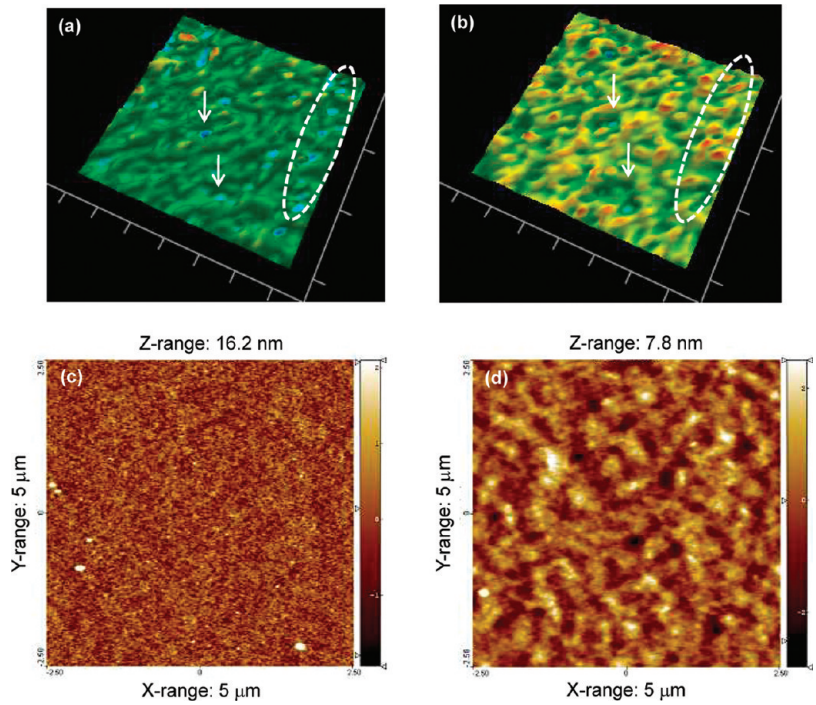

FIGURE 3. Surface characterization of the pNIPAM nanosheet. (a, b) IR images of the pNIPAM nanosheet (176 μm × 176 μm slice) for (a) 1650 cm^{-1} and (b) 1600 cm^{-1}. The arrows and dashed circles correspond to the same regions between (a) and (b). (c, d) AFM images of a pNIPAM nanosheet obtained (c) before and (d) after polymerization.

isopropyl and amide group of the pNIPAM brushes, although the asymmetric (1600 cm^{-1}) and symmetric (1400 cm^{-1}) stretches derived from the carboxylate anion group of the polysaccharide LbL film are hindered by the amide I carbonyl stretch of pNIPAM (Figure 2d). These results confirmed the growth of pNIPAM brushes from the polysaccharide nanosheets.

To estimate the molecular weight of the pNIPAM polymer with brushes, ATRP was carried out by adding a small amount of a free initiator to the reaction mixture. The use of the free initiator with ATRP has been shown to be advantageous in approximating the molecular weight of polymers (49, 50). Gel permeation chromatography (GPC) was performed for the free pNIPAM polymer grown from the free initiator after ATRP of the pNIPAM brushes. For 0.5 M NIPAM, a 10 μL portion of the free initiator (2-bromoisobutyric acid ethyl ester) was added to the reaction solution. After polymerization, the free pNIPAM polymer was purified by ion exchange (Amberlyst, 1:1 water/methanol) to remove Cu^{2+} ions. The product was precipitated with diethyl ether and lyophilized. Then, the lyophilized pNIPAM was dissolved in 50 mM LiCl in dimethyl formamide for GPC analysis. The GPC chromatograph showed the average M_n value of pNIPAM to be 85 000, although the polydispersity index (PDI) was approximately twice as high (PDI = 2.59) as that from our previous results (PDI; = 1.40) (Figure S2, Supporting Information), presumably because of the effect of the high monomer concentration used to build the condensed pNIPAM brushes. The addition of a free initiator during polymerization may reduce the overgrowth of pNIPAM brushes, resulting in well-controlled ATRP (50).

Surface Characterization of the pNIPAM Nanosheet. Formation of homogeneous pNIPAM brushes is essential to the production of a thermoresponsive surface. As FT-IR imaging is one of the most powerful tools for obtaining spatially and temporally resolved chemical and structural information (51, 52), we used this technique to analyze the macroscopic state of the pNIPAM brushes on the nanosheet. The images of the pNIPAM brushes sliced at 1650 cm^{-1} (Figure 3a) showed a preponderance of green signals of the amide I carbonyl backbone stretch, which originates in the pNIPAM brushes. However, these green signals were less apparent in certain regions of Figure 3a, such as the carboxylated regions indicated by reddish signals (i.e., dots indicated by arrows or dashed circle) in the slice at 1600 cm^{-1} (Figure 3b). We calculated the percentage of pNIPAM coverage from the green signals to be ca. 85%, which suggested that the growth of pNIPAM brushes was favored on the amine regions derived from chitosan in the polysaccharide LbL film.

The AFM images show the microscopic morphological differences in the nanosheet before and after polymerization at ambient temperature (room temperature). The nanosheet before polymerization has a very smooth surface, with a thickness of 44.7 nm and a surface roughness of 0.50 nm (rms (root-mean-square) value) (Figure 3c). In contrast, the surface of the pNIPAM nanosheet after polymerization is rougher, having homogeneous polymer brushes with a total film thickness of 107.6 nm and a surface roughness of 0.78 nm (rms value) (Figure 3d). Under the same ATRP conditions, the pNIPAM brushed surface was also obtained on a chitosan spin-coated monolayer surface with a thickness of 7.9 nm and a roughness of 1.9 nm (Figure S3, Supporting Information). However, the homogeneous growth of pNIPAM brushes was not obtained on this surface, because the number of reactive groups (−OH and −NH_2) for the bromo

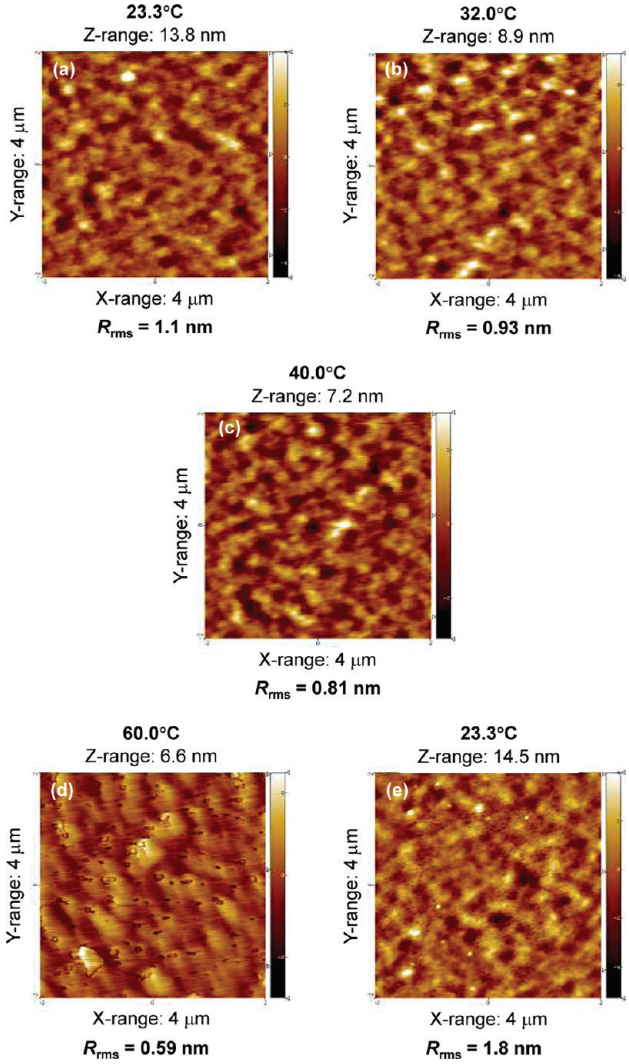

FIGURE 4. Stimuli-responsive surface of the pNIPAM nanosheet monitored under thermal temperature-driven in situ AFM scanning for stepwise increases of temperature: (a) 23.3 °C; (b) 32.0 °C; (c) 40.0 °C; (d) 60.0 °C; (e) decrease to 23.3 °C following (d).

initiation and ATRP is far less than in the multilayered polysaccharide LbL film. Therefore, the polysaccharide LbL film is quite a useful platform for the construction of polymer brushes.

Evaluation of the Thermoresponsive Surface of the pNIPAM Nanosheet. Temperature-driven in situ AFM scanning was utilized to evaluate the thermoresponsive properties of the pNIPAM nanosheet. This method was performed specifically to observe morphological changes at a constant position on the same sample surface undergoing an in situ temperature change. Morphological changes to the surface and roughness of the pNIPAM nanosheet were analyzed while the scanning region was fixed during observation. First, an initial rms roughness value of 1.1 nm was recorded at 23.3 °C. At 40.0 and 60.0 °C (higher than the LCST of pNIPAM, 32 °C), the rms values decreased to 0.81 and 0.59 nm, respectively (Figure 4). These results indicate that the surface morphology gets smoother with increasing temperature Moreover, the surface roughness was recovered (rms value 1.8 nm) after cooling to 23.3 °C. Caruso et al. (41) reported that the rms roughness of pNIPAM changed from 5−8 nm at 10−21 °C to 1−2 nm at 30 °C. Their results reveal the same general trend as our results: a decrease in surface roughness with an increase in temperature. However, the decrease in roughness in our experiments is less than that found by the Caruso groups. We suppose that this difference occurs because, in our case where the sample was in a dried state under ambient conditions, the pNIPAM brushes should be collapsed, compared to the fully swollen pNIPAM brushes in water measured by Caruso et al.

We also measured the mean water contact angle of the pNIPAM nanosheet by changing the temperature in a manner similar to that for the in situ AFM scanning. The mean contact angle of the pNIPAM nanosheet is 59 ± 8° at 25 °C. With an increase in temperature to 40 °C, the contact angle increased to 71 ± 2°. The initial angle was almost fully recovered (65 ± 3°) upon cooling to 25 °C (Figure S4, Supporting Information). Thus, we confirmed that the pNIPAM nanosheet on the substrate is thermoresponsive, induced by a swollen-to-unperturbed coil transition of pNIPAM brushes.

However, the variation in the contact angles measured here is 12° when the temperatue is increased from 25 to 40 °C, a smaller change than in our previous report (37) (45°) for pNIPAM brushes on an LbL film composed of poly(allylamine hydrochloride) (PAH) and poly(acrylic acid) (PAA). This difference can be attributed to the increased hydrophilicity of the underlying LbL film in the latter case, indicated by a contact angle of 20° for a LbL film of PAH and PAA. Okano et al. (40) reported that the contact angle of pNIPAM brushes on a polystyrene dish was 38° at 20 °C and 44° at 37 °C. This change in the contact angle of 6° means that pNIPAM brushes became more hydrophobic, influenced by the polystyrene substrate. Considering the fact that the contact angle of the polysaccharide LbL film is 62°, the hydrophobicity of the underlying substrate will influence the contact angle change of the pNIPAM brushes on the polysaccharide LbL film.

Evaluation of the Thermoresponsive Properties of the Freestanding pNIPAM Nanosheet. In general, the swollen-to-unperturbed coil transition of the pNIPAM brushes on the solid surface is a more gradual transition than that observed in a dilute aqueous solution, due to differences in the configuration of water molecules around the pNIPAM (7). Therefore, because of the increased accessibility of water to the pNIPAM, we would expect to observe an enhancement of the thermoresponsive properties of the pNIPAM brushes using a flexible freestanding pNIPAM nanosheet obtained by removal of the solid substrate. In order to peel the pNIPAM nanosheet from a SiO_2 substrate, a supporting film was employed in the form of a water-soluble PVA supporting film (43). Because the interaction between the pNIPAM nanosheet and the supporting film is stronger than that between the pNIPAM nanosheet and the SiO_2 substrate, this method allows for convenient collection of the freestanding nanosheet by peeling a dried bilayered film from the SiO_2 substrate. Afterward, the pNIPAM nanosheet can be released into aqueous solution by dissolution of the PVA

Table 1. Comparison of Physical Properties during a Freestanding Procedure

		elemental composition (%)		
	thickness	O	N	C
before PVA deposition	94 ± 4 nm	15.1	9.26	75.7
during PVA deposition	>70 μm	29.1	0.400	70.5
after PVA removal	90 ± 5 nm	13.3	11.2	75.6

film. During this procedure, we evaluated the PVA removal from the pNIPAM nanosheet by measuring the film thickness with a surface profilometer as well as the elemental composition by XPS (Table 1). From profilometry, we found that the thickness did not show a significant difference between the pNIPAM nanosheets before PVA deposition (94 ± 4 nm) and after PVA removal (90 ± 5 nm). From the XPS elemental analysis of C, N, and O, elemental composition between the pNIPAM nanosheets before PVA deposition and after PVA removal did not show the significant difference. In particular, the high-resolution XPS spectra of the C1s region showed an obvious difference as a result of the PVA deposition process (Figure S5, Supporting Information). The C−O peak (286 eV) corresponding to the PVA backbone can be seen in the PVA-coated pNIPAM nanosheet but cannot be seen in the pNIPAM nanosheets either before PVA deposition or after PVA removal. These results, therefore, confirmed that the PVA film was cleanly removed from the pNIPAM nanosheet.

Following the method shown in Figure 1, a 10 wt % polyvinyl alcohol (PVA) aqueous solution was cast on a pNIPAM nanosheet on an SiO_2 substrate. Then, the substrate was dried in vacuo until a solid PVA film was obtained. The resulting bilayered film is composed of an 88 nm thick pNIPAM nanosheet and a 70 μm thick PVA film, which was easily peeled off of the SiO_2 substrate by picking up the edge with tweezers (Figure 5a). The surface of the SiO_2 substrate is quite smooth (Figure 5b), and the rear of the nanosheet shows a mosaic structure (Figure 5c), composed of LbL assembled into domains with pNIPAM. These results suggest that the pNIPAM nanosheet is completely transferred to the PVA film with retention of the overall structure prepared on the SiO_2 substrate.

When the bilayered film was dropped into DI water, the PVA film dissolved and then the freestanding pNIPAM nanosheet appeared on the air−water interface. After the aqueous medium was exchanged three times with fresh DI water, the freestanding pNIPAM nanosheet had a pale blue color at 25 °C on the air−water interface and was slightly flexible with a creased surface (Figure 6a). As the water temperature was increased to 40 °C, the pNIPAM nanosheet turned yellow. Furthermore, the nanosheet lost its flexibility, which solidified at the air−water interface. Interestingly, this morphological transformation in color and flexibility with temperature at the air−water interface is reversible: the sheet is transparent pale blue with a flexible surface at 25 °C (Figure 6c) and cloudy yellow with a solid surface at 40 °C (Figure 6d) (see also Figure S6 in the Supporting Information). Consequently, we evaluated the reproducibility of this morphological transformation and confirmed it to be reproducible over at least over five cycles from 25 to 40 °C. Strikingly, the time required for the morphological transformation became shorter and shorter from over 30 s (first cycle) to a constant value of around 10 s (after the fourth cycle), which may correspond to the hydration of the pNIPAM nanosheet by the surrounding water through osmosis.

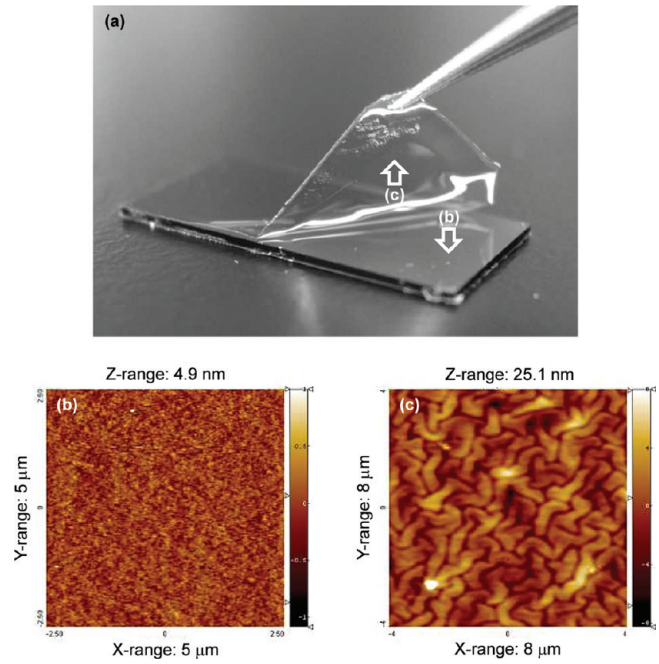

FIGURE 5. (a) Peeling off of the bilayered film using the supporting film method: macroscopic image of the bilayered film (1 cm × 2 cm) composed of the pNIPAM nanosheet and supporting PVA film being peeled away with tweezers. (b, c) AFM images of (b) the SiO_2 substrate after peeling off the PVA film and (c) the reverse side of the pNIPAM nanosheet.

In a previous study (45), we investigated the color of polysaccharide nanosheets and showed that structural color is principally a consequence of thickness. Therefore, the color changes in the free-standing pNIPAM nanosheet can be seen as an indicator of its changing thickness. An accurate estimation of the thickness was quite difficult in this experiment, because the refractive indexes and the optical thickness for the freestanding states of the pNIPAM nanosheet are required. Moreover, the pNIPAM nanosheets after collection on the SiO_2 substrate were highly swelled by water due to the formation of pNIPAM brushes. However, the surface roughness and surface wettability shown in Figure 4 and Figure S4 (Supporting Information) suggest that the surface morphology of the pNIPAM nanosheet and "swellability" were reversibly changed via the swollen-to-unperturbed coil transition of the pNIPAM brushes. This result could explain the morphological transformation of the freestanding nanosheets as follows: pNIPAM at 25 °C is extended and hydrophilic; therefore, the surface morphology of the pNIPAM nanosheet is flexible and transparent, bearing water molecules on the surface. On the other hand, pNIPAM at 40 °C is collapsed and hydrophobic; therefore, the surface morphology of the pNIPAM nanosheet is solid and cloudy, with hydrophobically organized pNIPAM brushes. Hence, the morphological transformations of the pNIPAM nanosheet

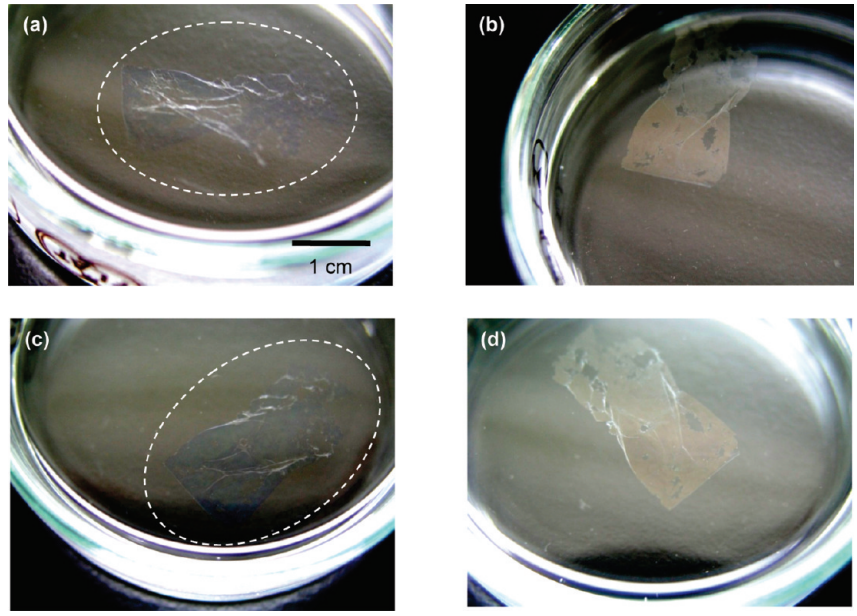

FIGURE 6. In situ morphological transformation of a freestanding pNIPAM nanosheet (1 cm × 2 cm) in water being warmed from (a) 25 °C to (b) 40 °C and then cooled to (c) 25 °C and heated again to (d) 40 °C.

are induced by the thermoresponsive properties of the pNIPAM brushes. As long as we observed the floating morphology of the freestanding polysaccharide nanosheets, with or without pNIPAM brushes, at ambient temperature, the nanosheets were stable and did not exhibit any swelling behaviors, such as an expansion of the structural dimension. However, when the temperature was increased, the polysaccharide nanosheet without pNIPAM brushes immediately sank into the water and never floated back up (*data not shown*). This could be due to the dissolution of polyelectrolyte, an effect that was prevented by the existence of hydrophobic pNIPAM brushes. Therefore, we propose that the freestanding nanosheet cannot undergo a morphological transformation without the presence of pNIPAM brushes, with their attendant phase transition behavior.

We further examined the effect of an anionic surfactant such as sodium *n*-dodecylsulfate (SDS) on the pNIPAM nanosheet and found that the interfacial hydrodynamics of pNIPAM are highly dependent on the concentration of SDS. Two different concentrations of an SDS medium were prepared around the critical micelle concentration (CMC = 8 mM) of SDS for dispersion of the pNIPAM nanosheet. For 16 mM over the CMC of SDS, the freestanding pNIPAM nanosheet gradually sank into the medium and was suspended. However, no morphological transformation was observed at this concentration, even when the temperature was increased from 25 to 40 °C. This suggests that the surface of the pNIPAM nanosheet is then covered with SDS micelles, reducing the thermoresponsive hydrodynamic behavior of the pNIPAM brushes. On the other hand, at 0.16 mM under the CMC of SDS, the pNIPAM nanosheet was stably suspended in the SDS medium at 25 °C (Figure 7a). Interestingly, the pNIPAM nanosheet gradually floated up upon gentle shaking of the glass dish and was finally localized at the air−water interface, turning yellow as the temperature was increased to 40 °C (Figure 7b).

This result strongly suggests that the SDS concentration in the medium is critical to controlling the hydrodynamics of the freestanding pNIPAM nanosheet. Previously, Napper et al. indicated the ability of SDS molecules to interact with pNIPAM brushes by varying the SDS concentration (53). They demonstrated that an SDS concentration over the CMC strongly interrupted the swollen-to-unperturbed coil transition of pNIPAM, due to the hydrophobic interaction of SDS molecules with the pNIPAM brushes. However, such a transition was not interrupted by the SDS molecules below the CMC. According to their results, a freestanding pNIPAM nanosheet can be suspended with the addition of SDS. In particular, the shape transformation of the pNIPAM nanosheet occurs so long as the SDS concentration is below the CMC because, while such a concentration enables the nanosheet to suspend, it does not interrupt the swollen-to-unperturbed coil transition of the pNIPAM brushes (Figure 7c). Quite recently, Kunitake et al. reported a similar effect of SDS, where they found that SDS assembled on the surface of freestanding ultrathin membranes (52). In general, pNIPAM undergoes shrink−stretch motion depending on the surrounding temperature. In our experiments, highly dense pNIPAM brushes also move unidirectionally in the film, an effect which was apparent in the in situ AFM experiments. Taking into account both of the previous reports, it appears that SDS can assemble and detach itself around the pNIPAM brushes on the polysaccharide nanosheet. In another words, it seems likely that the appropriate concentration of SDS will enhance the hydrodynamic behavior of the flexible pNIPAM nanosheets, powered not just by water convection induced by shaking but also by a change in the hydrophilic/phobic nature of the pNIPAM brushes.

Hence, an SDS concentration below the CMC is critical in enhancing the dynamic thermoresponsive behavior of the pNIPAM nanosheet by raising the temperature through the LCST. Microscopic changes in the mechanical properties of

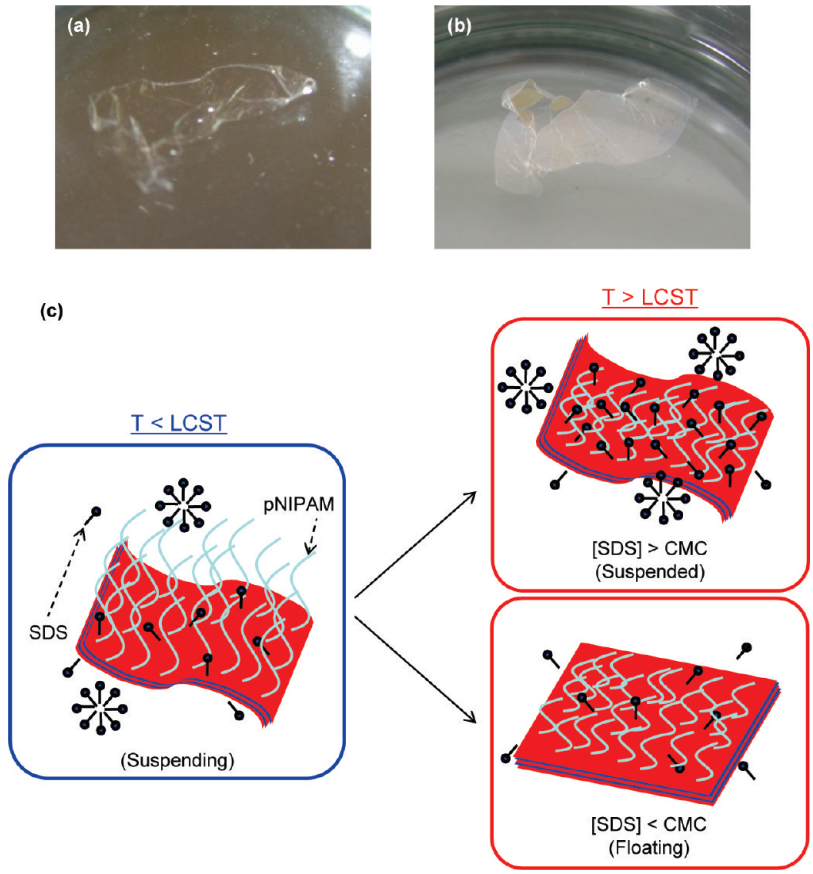

FIGURE 7. (a, b) Hydrodynamic effect of the anionic surfactant SDS on the pNIPAM nanosheet. The pNIPAM nanosheet (1 cm × 2 cm) (a) was suspended in water at 25 °C and (b) floated up to the air−water interface at 40 °C. (c) Scheme explaining the effect of anionic surfactants. The pNIPAM nanosheet was suspended at both 25 °C (<LCST) and 40 °C (>LCST) when the SDS concentration exceeded the critical micelle concentration (CMC). However, the pNIPAM nanosheet floated at 40 °C when the SDS concentration was below the CMC.

freestanding pNIPAM nanosheets are currently being investigated using an AFM force-indentation technique.

CONCLUSIONS

Ellipsometry, IR imaging, in situ temperature-controlled AFM, and contact angle measurements have confirmed the successful construction of thermoresponsive polymer brushes of pNIPAM on the surface of a polysaccharide nanosheet by the combination of an SA-LbL method, ATRP, and a water-soluble supporting film. A morphological transformation with temperature of the freestanding pNIPAM nanosheet was clarified through observation of a reversible color change on the air−water interface. Moreover, the thermoresponsive hydrodynamic behavior of the pNIPAM nanosheet causing the shape change was also observed by controlling the concentration of SDS. The freestanding polymer nanosheet is an attractive platform for building a stimuli-responsive surface, and such stimuli-responsive polymer brushes may also prove utility when applied to other functionalized surfaces (for example, pH, light, and magnetic field sensitive surfaces).

Acknowledgment. We thank Dr. K. Nagase at Tokyo Women Medical College for useful advice on GPC performance. This work was supported by the Global COE "Practical Chemical Wisdom" (T.F. and A.M.), "Consolidated Research Institute for Advanced Science and Medical Care" (S.T.), and "High-Tech Research Center" Project for Waseda University: matching fund subsidy from the MEXT of Japan. T.F. was a scholar "Doctor-21" of the Yoshida Scholarship Foundation.

Supporting Information Available: Figures giving an XPS spectrum of the pNIPAM nanosheet on SiO_2 substrate, a GPC chromatograph of pNIPAM polymer, AFM images of pNIPAM brushes on a chitosan spin coated film, the water contact angles of pNIPAM nanosheets, high-resolution XPS spectra of the C1s region for the pNIPAM nanosheet, and a morphological transformation of a freestanding pNIPAM nanosheet. This material is available free of charge via the Internet at http://pubs.acs.org.

REFERENCES AND NOTES

(1) Matyjaszewski, K.; Xia, J. *Chem. Rev.* **2001**, *101*, 2921–2990.
(2) Chang, D. P.; Dolbow, J. E.; Zauscher, S. *Langmuir* **2007**, *23*, 250–257.
(3) Kim, J. H.; Lee, T. R. *Drug Dev. Res.* **2006**, *67*, 61–69.
(4) Harnish, B.; Robinson, J. T.; Pei, Z. C.; Ramstrom, O.; Yan, M. D. *Chem. Mater.* **2005**, *17*, 4092–4096.
(5) Hiller, J.; Rubner, M. F. *Macromolecules* **2003**, *36*, 4078–4083.
(6) Rao, G. V. R.; Krug, M. E.; Balamurugan, S.; Xu, H. F.; Xu, Q.; Lopez, G. P. *Chem. Mater.* **2002**, *14*, 5075–5080.
(7) Park, M. K.; Deng, S.; Advincula, R. C. *J. Am. Chem. Soc.* **2004**, *126*, 13723–13731.
(8) Balamurugan, S.; Mendez, S.; Balamurugan, S. S.; O'Brien, M. J.; Lopez, G. P. *Langmuir* **2003**, *19*, 2545–2549.
(9) Ista, L. K.; Mendez, S.; Perez-Luna, V. H.; Lopez, G. P. *Langmuir* **2001**, *17*, 2552–2555.

(10) Lvov, Y.; Decher, G.; Möhwald, H. *Langmuir* **1993**, *9*, 481–486.
(11) Decher, G. *Science* **1997**, *277*, 1232–1237.
(12) *Multilayer Thin Films: Sequential Asssembly of Nanocompsoite Materials*; Decher, G., Schlenhoff, J. B., Eds.; Wiley-VCH: Weinheim, Germany, 2003.
(13) Serizawa, T.; Tamaguchi, M.; Akashi, M. *Biomacromolecules* **2002**, *3*, 724–731.
(14) Sano, K.; Sasaki, H.; Shibata, K. *J. Am. Chem. Soc.* **2006**, *128*, 1717–1722.
(15) Kotov, N. A.; Meldrum, F. C.; Fendler, J. H.; Tombacz, E.; Dekany, I. *Langmuir* **1994**, *10*, 3797–3804.
(16) Lvov, Y.; Ariga, K.; Ichinose, I.; Kunitake, T. *J. Am. Chem. Soc.* **1995**, *117*, 6117–6123.
(17) Decher, G.; Lvov, Y.; Schmitt, J. *Thin Solid Films* **1994**, *244*, 772–777.
(18) Tsukruk, V. V.; Bliznyuk, V. N.; Visser, D.; Campbell, A. L.; Buning, T. J.; Adams, W. W. *Macromolecules* **1997**, *30*, 6615–6625.
(19) Zhai, L.; Cobeci, F. C.; Cohen, R. E.; Rubner, M. F. *Nano Lett.* **2004**, *4*, 1349–1353.
(20) Jiang, C.; Tsukruk, V. V. *Adv. Mater.* **2006**, *18*, 829–840.
(21) Tang, Z.; Wang, Y.; Podsiadlo, P.; Kotov, N. A. *Adv. Mater.* **2006**, *18*, 3203–3224.
(22) Caruso, F.; Caruso, R. A.; Mohwald, H. *Science* **1998**, *282*, 1111–1114.
(23) Gao, C.; Moya, S.; Donath, E.; Mohwald, H. *Macromol. Chem. Phys.* **2002**, *203*, 953–960.
(24) Cortez, C.; Tomaskovic-Crook, E.; Johnston, A. P. R.; Radt, B.; Cody, S. H.; Scott, A. M.; Nice, E. C.; Heath, J. K.; Caruso, F. *Adv. Mater.* **2006**, *18*, 1998–2003.
(25) Mamedov, A. A.; Kotov, N. A. *Langmuir* **2000**, *16*, 5530–5533.
(26) Ono, S. S.; Decher, G. *Nano Lett.* **2006**, *6*, 592–598.
(27) Kado, Y.; Mitsuishi, M.; Miyashita, T. *Adv. Mater.* **2005**, *17*, 1857–1861.
(28) Jiang, C.; Markutsya, S.; Tsukruk, V. V. *Adv. Mater.* **2004**, *16*, 157–161.
(29) Jiang, C.; Markutsya, S.; Pikus, Y.; Tsukruk, V. V. *Nat. Mater.* **2004**, *3*, 721–728.
(30) Markutuya, S.; Jiang, C.; Pikus, Y.; Tsukruk, V. V. *Adv. Funct. Mater.* **2005**, *15*, 771–780.
(31) Cho, J.; Char, K.; Hong, J.; Lee, K. *Adv. Mater.* **2001**, *13*, 1076–1078.
(32) Cho, J.; Char, K. *Langmuir* **2004**, *20*, 4011–4016.
(33) Lin, Y.-H.; Jiang, C.; Xu, J.; Lin; Tsukruk, V. V. *Adv. Mater.* **2008**, *19*, 3827–3832.
(34) Endo, H.; Kado, Y.; Mitsuishi, M.; Miyashita, T. *Macromolecules* **2006**, *39*, 5559–5563.
(35) Vendamme, R.; Onoue, S.; Nakao, A.; Kunitake, T. *Nat. Mater.* **2006**, *5*, 494–501.
(36) *Polymer Brushes: Synthesis, Characterization, Applications*; Advincula, R. C., Brittain, W. J., Caster, K. C., Rühe, J., Eds.; Wiley-VCH: Weinheim, Germany, 2004.
(37) Fulghum, T. M.; Estillore, N. C.; Vo, C.-D.; Armes, S. P.; Advincula, R. C. *Macromoleucles* **2008**, *41*, 429–435.
(38) Uhlmann, P.; Ionov, L.; Houbenov, N.; Nitschke, M.; Grundke, K.; Motornov, M.; Minko, S.; Stamm, M. *Prog. Org. Coat.* **2006**, *55*, 168–174.
(39) Takeoka, S.; Okamura, Y.; Fujie, T.; Fukui, Y. *Pure Appl. Chem.* **2008**, *80*, 2259–2271.
(40) Fujie, T.; Matsutani, N.; Kinoshtia, M.; Okamura, Y.; Saito, A.; Takeoka, S. *Adv. Funct. Mater.*, in press (DOI: 10.1002/adfm.(200900103)).
(41) Mizutani, A.; Kikuchi, A.; Yamato, M.; Kanazawa, H.; Okano, T. *Biomaterials* **2008**, *29*, 2073–2081.
(42) Quinn, J. F.; Caruso, F. *Langmuir* **2004**, *20*, 20–22.
(43) Li, M.-H.; Keller, P.; Yang, J.; Albouy, P.-A. *Adv. Mater.* **2004**, *16*, 1922–1925.
(44) Fujie, T.; Okamura, Y.; Takeoka, S. *Adv. Mater.* **2007**, *19*, 3549–3553.
(45) Fujie, T.; Okamura, Y.; Takeoka, S. *Colloids Surf., A* **2009**, *334*, 28–33.
(46) Carlmark, A.; Malmström, E. *J. Am. Chem. Soc.* **2002**, *124*, 900–901.
(47) Singh, N.; Wang, J.; Ulbricht, M.; Wickramasinghe, S. R.; Husson, S. C. *J. Membr. Sci.* **2008**, *309*, 64–72.
(48) Stroock, A. D.; Kane, R. S.; Weck, M.; Metallo, S. J.; Whitesides, G. M. *Langmuir* **2003**, *19*, 2466–2472.
(49) Fulghum, T. M.; Patton, D. L.; Advincula, R. C. *Langmuir* **2006**, *22*, 8397–8402.
(50) Tsuji, Y.; Ohno, K.; Yamamoto, S.; Goto, A.; Fukuda, T. *Adv. Polym. Sci.* **2006**, *197*, 1–45.
(51) Bae, W.-O.; Urban, M. W. *Biomacromolecules* **2006**, *7*, 1156–1161.
(52) Miller-Chou, B. A.; Koenig, J. L. *Macromolecules* **2003**, *36*, 4851–4861.
(53) Zhu, P. W.; Napper, D. H. *Langmuir* **1996**, *12*, 5992–5998.
(54) Vendamme, R.; Kunitake, T. *Soft Matter* **2008**, *4*, 797–804.

AM900111R